

## CHAPTER 2

### THEORY

Using atomic PNC to test the standard model brings together two disparate fields of physics: high-energy physics and atomic physics. It is not the purpose of this chapter to write at length about the underlying theories. Instead, this chapter presents enough theory so that the atomic physics measurements can be understood, and it also illustrates the way in which the measurements provide a test of the standard model. The theory of the weak interaction is covered in detail in the literature, and the reader is referred there for technical details and for general information on atomic theory [16, 17, 18, 19]. Here only an overview will be provided.

This chapter covers the theory necessary to understand the experiments discussed and the implications of those experiments. In addition to the general theory, this chapter also covers the effects of external magnetic fields and their alignment with respect to the experimental apparatus, and it details the exact transition rates the experiments measure. Much of the content of this chapter closely follows the theses of Gilbert [20], Noecker [21], Masterson [22], and Wood [23].

#### 2.1 Weak Interaction

The weak interaction can be mediated by the exchange of a  $Z^0$  boson between an electron and a quark. This exchange, shown in Fig. 1.2(b), is analogous to the exchange of a photon for the electromagnetic interaction, shown in Fig. 1.2(a). In the present form of the standard model, the weak interaction is described by a

Hamiltonian given by

$$H_{\text{PNC}} = \frac{1}{2\sqrt{2}} G_F Q_W \gamma^5 \rho_N(r), \quad (2.1)$$

where  $G_F$  is the Fermi constant,  $\rho_N(r)$  is the nuclear density, and  $\gamma^5$  is the Dirac matrix, which is responsible for PNC. The weak charge of the nucleus,  $Q_W$ , is analogous to the electric charge for the electromagnetic interaction. For an atom with atomic number  $Z$  and  $N$  neutrons, the value of  $Q_W$  is given by

$$Q_W = 2[(2Z + N)C_{1u} + (Z + 2N)C_{1d}], \quad (2.2)$$

where  $C_{1u}$  and  $C_{1d}$  are electron-quark coupling constants for the up and down quarks, respectively, which are described in Chapter 1. Thus,  $Q_W$  is atomic physics' "window" into the standard model. At tree level\*  $Q_W$  is given by

$$Q_W = -(N - Z + 4 \sin^2 \theta_W), \quad (2.3)$$

where  $\sin^2 \theta_W$  is the Weinberg angle. Any deviation from the tree level value of  $Q_W$  indicates the need for higher order corrections (such as the so-called "radiative corrections") or signals a breakdown in the standard model predictions.

The weak interaction does not conserve parity, so  $H_{\text{PNC}}$  mixes states of opposite parity as in

$$|\overline{\psi}\rangle = |\psi^+\rangle + \sum_i |\phi_i^-\rangle \frac{\langle \phi_i^- | H_{\text{PNC}} | \psi^+ \rangle}{E_\psi - E_{\phi_i}} \quad (2.4)$$

where the "+" and "-" indicate opposite parity states. The matrix elements  $\langle \phi_i^- | H_{\text{PNC}} | \psi^+ \rangle$  are essentially matrix elements of  $\gamma^5$ . The operator  $\gamma^5$  does not appear in any atomic observable, so the values of these matrix elements must be calculated. The

---

\*Tree level is essentially the lowest order of the theory.

Bouchiat [8] have shown that in the non-relativistic approximation

$$\langle n'\ell' | H_{\text{PNC}} | n\ell \rangle \propto \left( R_{n'\ell'}(r) \frac{\partial R_{n\ell}(r)}{\partial r} \right) \Big|_{r=0}, \quad (2.5)$$

where  $n$  is the principal quantum number,  $\ell$  is the orbital angular momentum quantum number, and  $R_{n\ell}(r)$  is the radial wave function of the  $|n\ell\rangle$  state. Because  $R_{n\ell}(r) \approx r^\ell Z^{\ell+\frac{1}{2}}$  for small  $r$ ,  $H_{\text{PNC}}$  mixes only  $S$  and  $P$  states, and to a good approximation it only mixes states with  $J = 1/2$ .

## 2.2 Cesium Energy Level Structure.

Atomic cesium has a single valence electron with a Xenon-like core. We use the stable isotope  $^{133}\text{Cs}$ , which has 55 protons and 78 neutrons. It has nuclear spin  $I = 7/2$ , electronic spin  $S = 1/2$ , orbital angular momentum  $L = 0, 1, \dots$ , and total electronic angular momentum  $\vec{J} = \vec{L} + \vec{S}$ . Its total angular momentum is given by  $\vec{F} = \vec{I} + \vec{J}$ , so with  $J = 1/2$  there are two hyperfine levels:  $F = 3$  and 4. With  $J = 3/2$  there are four hyperfine levels:  $F = 2, 3, 4$ , and 5. The projection of  $F$  onto the quantization axis is given by  $m_F = -F, -F + 1, \dots, F - 1, F$ . The most important of these energy levels are shown in Fig. 2.1.

Perhaps the most familiar spectral features of atomic cesium are the so-called ‘‘D1’’ and ‘‘D2’’ lines, which are electric dipole transitions from the  $6S_{1/2}$  ground state to the  $6P_{1/2}$  and  $6P_{3/2}$  states, respectively. The work in this thesis uses the D2 line for optical pumping and for detection, and it uses the normally forbidden transition between the  $6S_{1/2}$  and  $7S_{1/2}$  states to study the interesting science.

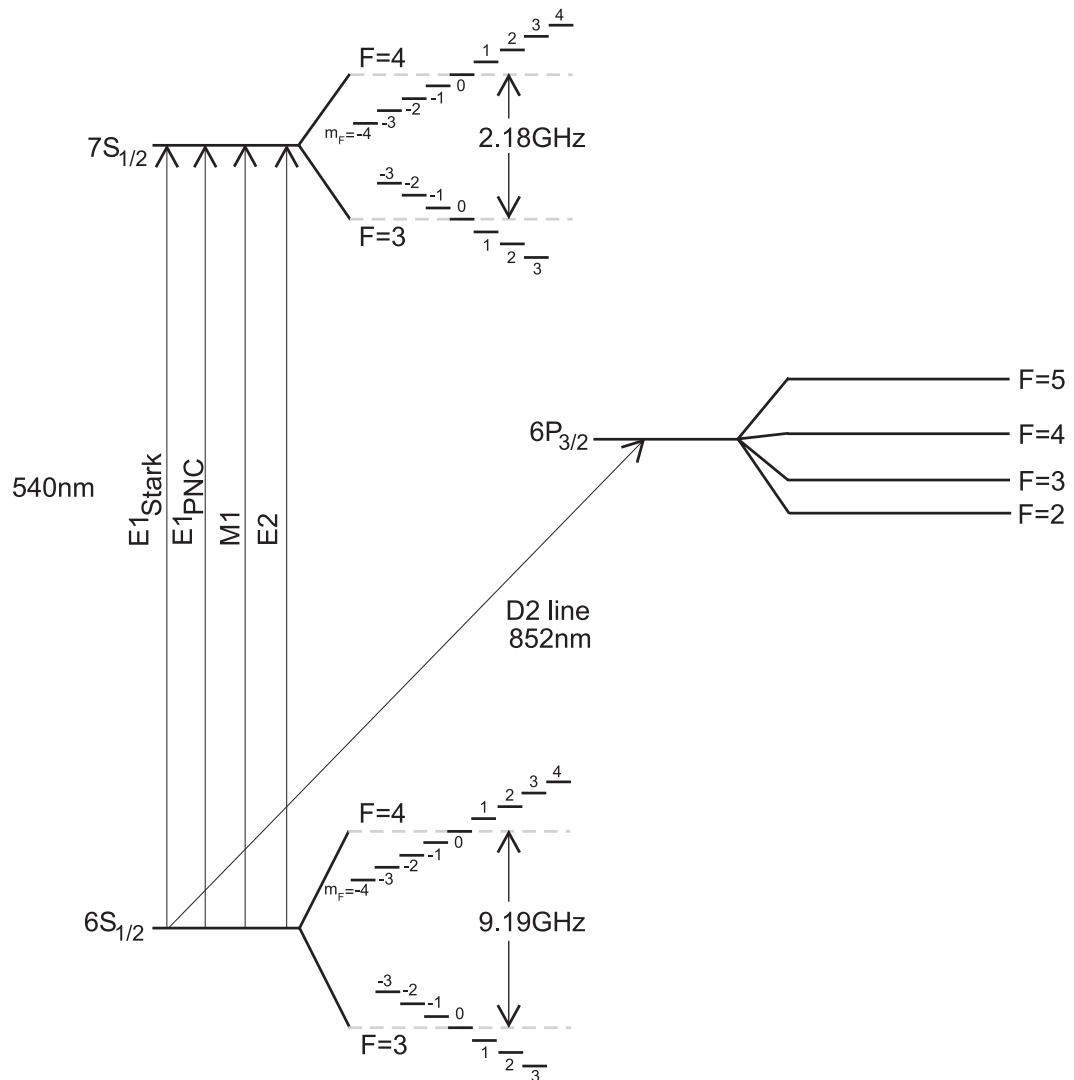


Figure 2.1: The lowest energy levels of the cesium atom. The mechanisms giving rise to the  $6S \rightarrow 7S$  transition are shown, as well as hyperfine structure of all the states and the Zeeman structure of the  $6S$  and  $7S$  states. The  $6P_{1/2}$  state is not shown because of its relative unimportance for the work presented in this thesis. Energy splittings are not shown to scale in this figure.

## 2.3 Electric Dipole Amplitudes

### 2.3.1 Parity Nonconserving Amplitude

In cesium, the mixing of  $S$  and  $P$  states by the weak interaction discussed in Section 2.1 is given by

$$\overline{|nSFm_F\rangle} = |nSFm_F\rangle + \sum_{n'} |n'P\rangle \frac{\langle n'P | H_{\text{PNC}} | nSFm_F\rangle}{E_{nS} - E_{n'P}}. \quad (2.6)$$

In the presence of an oscillating laser field with electric field polarization  $\vec{\epsilon}$ , there is an  $E1$  amplitude between the  $6S$  and  $7S$  states of cesium. This amplitude is given by

$$\begin{aligned} (E1_{\text{PNC}})_{Fm_F}^{F'm'_F} &= \overline{\langle 7SF'm'_F | -e\vec{\epsilon} \cdot \vec{r} | 6SFm_F \rangle} \\ &= \sum_n \left( \frac{\langle 7SF'm'_F | H_{\text{PNC}} | nP \rangle \langle nP | \vec{D} | 6SFm_F \rangle}{E_{7S} - E_{nP}} \right. \\ &\quad \left. + \langle 7SF'm'_F | \vec{D} | nP \rangle \frac{\langle nP | H_{\text{PNC}} | 6SFm_F \rangle}{E_{6S} - E_{nP}} \right) \\ &= i\text{Im}(E_{\text{PNC}})\vec{\epsilon} \cdot \langle F'm'_F | \vec{\sigma} | Fm_F \rangle, \end{aligned} \quad (2.7)$$

where the unprimed quantum numbers are for the ground state and the primed quantum numbers are for the excited state, and the operator  $\vec{\sigma}$  is the Pauli spin matrix. The constant  $E_{\text{PNC}}$  contains all the radial information as well as the connection to the standard model:

$$E_{\text{PNC}} = \sum_n \left( \frac{\langle 7S | H_{\text{PNC}} | nP \rangle \langle nP | \vec{D} | 6S \rangle}{E_{7S} - E_{nP}} + \frac{\langle 7S | \vec{D} | nP \rangle \langle nP | H_{\text{PNC}} | 6S \rangle}{E_{6S} - E_{nP}} \right). \quad (2.8)$$

$$(2.9)$$

the geometrical matrix element  $\langle F'm'_F | \vec{\sigma} | Fm_F \rangle$  can be written in terms

of the  $C_{Fm_F}^{F'm'_F}$  coefficients:

$$C_{Fm_F}^{F'm_F+q} \equiv \left(\frac{1}{\sqrt{2}}\right)^{|q|} \langle F'm_F+q | \sigma_{1q} | Fm_F \rangle, \quad (2.10)$$

where  $q = 0, \pm 1$ . These coefficients are simply combinations of Clebsch-Gordan coefficients, and they are tabulated in Appendix A. The PNC amplitude can then be written as

$$(E1_{\text{PNC}})_{Fm_F}^{F'm'_F} = i\text{Im}(E_{\text{PNC}}) [(\mp\epsilon_x + i\epsilon_y) \times C_{Fm_F}^{F'm_F\pm 1} \delta_{m_F m'_F \mp 1} + \epsilon_z C_{Fm_F}^{F'm_F} \delta_{mm'}], \quad (2.11)$$

where we have evaluated the dot product  $\vec{\epsilon} \cdot \vec{\sigma}$  in Eq. (2.7). Note that the operators  $\sigma_x$  and  $\sigma_y$  drive  $\Delta m_F = \pm 1$  transitions and  $\sigma_z$  drives  $\Delta m_F = 0$  transitions.

### 2.3.2 Stark-Induced Amplitude

An applied external dc electric field  $\vec{E}$  polarizes the cesium atom and also mixes states in a similar way the weak interaction does in Eq. (2.4) with  $H_{\text{PNC}}$  replaced with  $e\vec{E} \cdot \vec{r}$ . An oscillating laser field then drives the Stark-induced  $6S \rightarrow 7S$  amplitude given by

$$(E1_{\text{Stark}})_{Fm_F}^{F'm'_F} = \sum_{n,J,F'',m''_F} \left\{ \frac{\langle 7SF'm'_F | e\vec{E} \cdot \vec{r} | nP_J F'' m''_F \rangle \langle nP_J F'' m''_F | e\vec{\epsilon} \cdot \vec{r} | 6SFm_F \rangle}{E_{7S} - E_{nP_J}} + \frac{\langle 7SF'm'_F | e\vec{\epsilon} \cdot \vec{r} | nP_J F'' m''_F \rangle \langle nP_J F'' m''_F | e\vec{E} \cdot \vec{r} | 6SFm_F \rangle}{E_{7S} - E_{nP_J}} \right\}. \quad (2.12)$$

The Bouchiat [8] showed that this complicated expression can be written in a simple form using an effective dipole operator:

$$\begin{aligned} (E1_{\text{Stark}})_{Fm_F}^{F'm'_F} &= \vec{\epsilon} \cdot \langle 7SF'm'_F | \vec{r}_{\text{effective}} | 6SFm_F \rangle \\ &= \alpha \vec{E} \cdot \vec{\epsilon} \delta_{F,F'} \delta_{m_F m'_F} + i\beta \vec{\epsilon} \cdot \langle F'm'_F | \vec{\sigma} \times \vec{E} | Fm \rangle \\ &= \alpha \vec{E} \cdot \vec{\epsilon} \delta_{F,F'} \delta_{m_F m'_F} + i\beta (\vec{E} \times \vec{\epsilon}) \cdot \langle F'm'_F | \vec{\sigma} | Fm \rangle. \end{aligned} \quad (2.13)$$

Here  $\alpha$  and  $\beta$  are the scalar and tensor transition polarizabilities, respectively. They are given by [8, 24]

$$\begin{aligned} \alpha &= \frac{e^2}{9} \sum_n \left[ \langle 7S | r | nP_{1/2} \rangle \langle nP_{1/2} | r | 6S \rangle \left( \frac{1}{E_{7S} - E_{nP_{1/2}}} + \frac{1}{E_{6S} - E_{nP_{1/2}}} \right) \right. \\ &\quad \left. + 2 \langle 7S | r | nP_{3/2} \rangle \langle nP_{3/2} | r | 6S \rangle \left( \frac{1}{E_{7S} - E_{nP_{3/2}}} + \frac{1}{E_{6S} - E_{nP_{3/2}}} \right) \right], \end{aligned} \quad (2.14)$$

and

$$\begin{aligned} \beta &= \frac{e^2}{9} \sum_n \left[ \langle 7S | r | nP_{1/2} \rangle \langle nP_{1/2} | r | 6S \rangle \left( \frac{1}{E_{7S} - E_{nP_{1/2}}} - \frac{1}{E_{6S} - E_{nP_{1/2}}} \right) \right. \\ &\quad \left. - \langle 7S | r | nP_{3/2} \rangle \langle nP_{3/2} | r | 6S \rangle \left( \frac{1}{E_{7S} - E_{nP_{3/2}}} - \frac{1}{E_{6S} - E_{nP_{3/2}}} \right) \right]. \end{aligned} \quad (2.15)$$

The  $\Delta F = 0$  transitions are dominated by the  $\alpha$  term because  $\alpha/\beta = -9.905(11)$  [25]. Here  $\langle nS | r | nP \rangle$  are effective radial integrals which are related to reduced matrix elements by [24]

$$\langle nS || r || n'P_{1/2} \rangle = \langle n'P_{1/2} || r || nS \rangle = \sqrt{\frac{2}{3}} \langle nS | r | n'P_{1/2} \rangle \quad (2.16)$$

and

$$\langle nS || r || n'P_{3/2} \rangle = -\langle n'P_{3/2} || r || nS \rangle = \sqrt{\frac{4}{3}} \langle nS | r | n'P_{3/2} \rangle. \quad (2.17)$$

We use these forms of Eqs. (2.14) and (2.15) to emphasize the fact that  $\alpha$  is the **sum** of similar sized terms and  $\beta$  is the **difference** of similar sized terms. Thus, the fractional uncertainty of  $\alpha$  is comparable to or better than the fractional uncertainty of its individual terms, while the fractional uncertainty of  $\beta$  is much worse than that of its individual terms.

If we evaluate the dot product as before, the Stark-induced amplitude can

be written as

$$\begin{aligned}
(E1_{\text{Stark}})_{Fm_F}^{F'm'_F} &= \alpha \vec{E} \cdot \vec{\epsilon} \delta_{FF'} \delta_{m_F m'_F} + i\beta (\vec{E} \times \vec{\epsilon})_z C_{Fm_F}^{F'm'_F} \delta_{m_F m'_F} \\
&+ \beta [\mp i (\vec{E} \times \vec{\epsilon})_x - (\vec{E} \times \vec{\epsilon})_y] C_{Fm_F}^{F'm'_F \pm 1} \delta_{m_F m'_F \mp 1}.
\end{aligned} \tag{2.18}$$

The Stark-induced and PNC electric dipole amplitudes differ significantly in size. If the D1 amplitude has a strength on the order of unity,  $E1_{\text{Stark}}$  has a strength of  $3 \times 10^{-5}$  when  $E = 500$  V/cm, and  $E1_{\text{PNC}}$  has a strength of  $10^{-11}$ .

## 2.4 Magnetic Dipole Amplitudes

Although to first order magnetic dipole ( $M1$ ) amplitudes vanish between states with different  $n$ , relativistic effects [26] and the off-diagonal hyperfine interaction [8] both contribute to a small amplitude between the  $6S$  and  $7S$  states. The Hamiltonian for this interaction connecting  $S$  states is given by

$$H_{M1} = \vec{\mu} \cdot \vec{B}_{\text{ac}} = \frac{\mu_B}{\hbar} (\hat{L} + 2\hat{S}) \cdot \vec{B}_{\text{ac}} \tag{2.19}$$

$$= \mu_B \vec{\sigma} \cdot \vec{B}_{\text{ac}} \tag{2.20}$$

where  $\mu_B$  is the Bohr magneton,  $\vec{\sigma} = 2\hat{S}/\hbar$  is the Pauli spin operator, and if  $\vec{k}$  is the propagation vector of the laser,  $\vec{B}_{\text{ac}} = \vec{k} \times \vec{\epsilon}$  is the oscillating magnetic field of the laser.  $\hat{L}$  and  $\hat{S}$  are the electron angular momentum and spin operators, respectively. The amplitude for the  $M1$  transition is then given by

$$M1_{Fm_F}^{F'm'_F} = \langle 7SF'm'_F | H_{M1} | 6SFm_F \rangle = M1(\vec{k} \times \vec{\epsilon}) \cdot \langle F'm'_F | \vec{\sigma} | Fm_F \rangle, \tag{2.21}$$

where the radial integrals have been incorporated into the constant  $M1$ . The radial part can be written as

$$M1 = M \pm M_{\text{hf}} \delta_{F, F' \pm 1}, \tag{2.22}$$

where  $M$  is from relativistic effects, and  $M_{\text{hf}}$  is from the off-diagonal hyperfine interaction. The  $M1$  amplitude has a size of about  $2 \times 10^{-6}$  compared with the D1 line. As before, Eq. (2.21) can be written as

$$M1_{Fm_F}^{F'm'_F} = M1\{[\mp(\vec{k} \times \vec{\epsilon})_x + i(\vec{k} \times \vec{\epsilon})_y] \\ \times C_{Fm_F}^{F'm_F \pm 1} \delta_{m_F m'_F \mp 1} + (\vec{k} \times \vec{\epsilon})_z C_{Fm_F}^{F'm_F} \delta_{m_F m'_F}\}. \quad (2.23)$$

## 2.5 Electric Quadrupole Interaction

Another transition that is driven by a laser field is the electric quadrupole transition ( $E2$ ), which arises from mixing of  $\langle n'D \rangle$  states with  $\langle n'S \rangle$  states by the off-diagonal hyperfine interaction. This amplitude is very small compared to the allowed  $E1$  transitions and even the  $M1$  transition ( $E2/M \approx 0.01$ ). However, in order to test the standard model at the few tenths of a percent level, we must account for the small effects of the  $E2$  amplitude, as discussed in Section 5.4 and Appendix B. In our case, the  $E2$  amplitude requires us to correct our data by only  $\sim 0.08\%$ ; in other experiments the necessary correction is as large as  $3\%$  [27]. Because the effect of  $E2$  on our measurements is so small, we can determine the ratio  $E2/M_{\text{hf}}$  by comparing our result for  $M_{\text{hf}}/M$  with other results that were affected by  $E2$ . See, for example, Ref. [28] and Section 5.4. A phenomenological discussion of  $E2$  following the treatment of Ref. [29] will be presented in Section 5.4.

## 2.6 Effect of Misaligned $\vec{B}$

In the foregoing discussion it has been assumed that the quantization axis is along  $\hat{z}$ . It is important to ask what happens if the magnetic field is slightly misaligned from the  $\hat{z}$  axis.

The effect of a misaligned magnetic field is to change the definition of the operator  $\vec{\sigma}$ . The Pauli spin matrix is defined assuming a quantization axis along  $\hat{z}$ , so we must rotate  $\vec{\sigma}'$ , which is defined with  $\vec{B} = B\hat{z}'$ , into the experimental

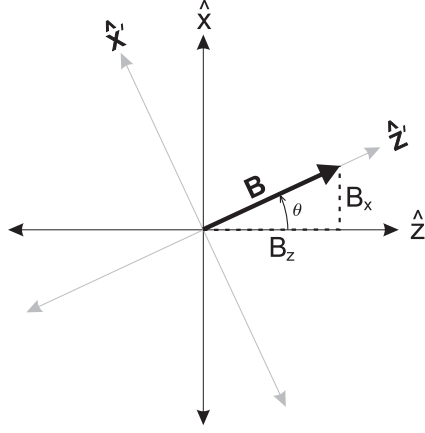


Figure 2.2: A picture showing magnetic field misaligned into the  $\hat{x}$  direction.

coordinate system where  $\vec{B} = B_x \hat{x} + B_y \hat{y} + B_z \hat{z}$ . Using Fig. 2.2 it is easy to see that  $\hat{z} = \cos \theta \hat{z}' - \sin \theta \hat{x}'$  and  $\hat{x} = \sin \theta \hat{z}' + \cos \theta \hat{x}'$ , where  $\cos \theta = B_z/B$  and  $\sin \theta = B_x/B$ . A similar rotation can be performed if  $\hat{y}$  replaces  $\hat{x}$  in the formulas. The components of the Pauli spin matrix are then given by

$$\begin{aligned}\sigma_x &= \frac{B_z}{B} \sigma'_x + \frac{B_x}{B} \sigma'_z \\ \sigma_y &= \frac{B_z}{B} \sigma'_y + \frac{B_y}{B} \sigma'_z \\ \sigma_z &= \frac{B_z}{B} \sigma'_z - \frac{B_x}{B} \sigma'_x - \frac{B_y}{B} \sigma'_y.\end{aligned}\tag{2.24}$$

Simple algebra then shows that the  $C_{Fm_F}^{F'm'_F}$  coefficients are transformed into

$$C_{Fm_F}^{F'm'_F \pm 1} \delta_{m_F m'_F \mp 1} \rightarrow C_{Fm_F}^{F'm'_F \pm 1} \delta_{m_F m'_F \mp 1} \mp \left( \frac{B_x}{B} \pm i \frac{B_y}{B} \right) C_{Fm_F}^{F'm'_F} \delta_{m_F m'_F}.\tag{2.25}$$

This means that a misaligned magnetic field introduces  $\Delta m_F = 0$  transitions where there should only be  $\Delta m_F = \pm 1$  transitions. The form of  $C_{Fm_F}^{F'm'_F} \delta_{m_F m'_F}$  is also changed, but it is not important for our purposes and so it is omitted.

## 2.7 Measured Transition Rates

As we have seen, in the presence of an external dc electric field and a cw laser field there are five different amplitudes connecting the  $6S$  and  $7S$  states of cesium: the PNC and Stark-induced  $E1$  amplitudes, the  $M1$  amplitudes from relativistic effects and off-diagonal hyperfine interactions, and the tiny  $E2$  amplitude. There are four hyperfine components to the  $6S \rightarrow 7S$  transition: the  $\Delta F = 0$   $F = 3$  to  $F' = 3$  and  $F = 4$  to  $F' = 4$ , and the  $\Delta F = \pm 1$   $F = 3$  to  $F' = 4$  and  $F = 4$  to  $F' = 3$ . All the experiments discussed in this thesis use  $\vec{E} = E\hat{x}$ ,  $\vec{B} = B\hat{z}^*$ , and  $\vec{k} = \hat{y}$ , and a general normalized polarization  $\vec{\epsilon} = \epsilon_z\hat{z} + (\epsilon_x + i\epsilon_i)\hat{x}$ .

The most recent PNC measurement performed by our group measured the interference between the Stark-induced and PNC electric dipole amplitudes. The geometry in that experiment used  $E \simeq 500$  V/cm,  $B \simeq 6.6$  G,  $\epsilon_i/\epsilon_z \simeq 1$  and  $2$ , and  $\epsilon_x = 0$ . The final quantity measured was the ratio of the two amplitudes for  $\Delta F = \pm 1$  transitions given by\*\*

$$R_{Fm_F}^{F'm'_F} = 2 \frac{\text{Im}(E_{\text{PNC}})}{\beta E} \frac{\epsilon_i}{\epsilon_z} \frac{\sum_{m_F} \pm f_{m_F} d_{m_F} \left(C_{Fm_F}^{F'm_F \pm 1}\right)^2}{\sum_{m_F} f_{m_F} d_{m_F} \left(C_{Fm_F}^{F'm_F \pm 1}\right)^2}, \quad (2.26)$$

where  $f_{m_F}$  is the fractional population in a Zeeman sublevel  $m_F$ ,  $d_{m_F}$  is a detuning factor that accounts for the non-degeneracy of different Zeeman transitions (see Section 2.8). The value  $\text{Im}(E_{\text{PNC}})/\beta$  can then be extracted if all the other quantities are measured.

In order to measure the dc Stark shift (see Chapter 2.18) we use the  $F = 3$  to  $F' = 3$  transition. We use electric fields from 1 kV/cm to 10 kV/cm, with  $\vec{E} = E\hat{x}$ ,

---

\*In this section we ignore the problem of misaligned magnetic fields. That will be addressed in Chapter 5

\*\*Actually, the ratios measured on the  $\Delta F = \pm 1$  transitions are slightly different because of nuclear PNC. This difference will be ignored in this thesis.

$B = 0$ , and  $\vec{\epsilon} = \epsilon_x \hat{x} + \epsilon_z \hat{z}$ . The transition rate from Eq. (2.12) is simply

$$| (E1_{\text{Stark}})_{Fm_F}^{Fm'_F} |^2 \simeq [\alpha^2 E^2 \epsilon_x^2 \delta_{m_F m'_F} + \beta^2 E^2 \epsilon_z^2 (C_{Fm_F}^{Fm'_F})^2 \delta_{m_F m'_F \pm 1}] \Lambda^{E1}(I, \nu), \quad (2.27)$$

where  $\Lambda^{E1}(I, \nu)$  is a line shape factor that depends on the intensity  $I$  and frequency  $\nu$  of the excitation laser (see Ref. [30]), and the small  $M1$  and  $E2$  rates have been ignored.

To measure the tensor transition polarizability  $\beta$  we use the  $\Delta F = \pm 1$  transitions. We also have  $E = 700$  and  $0$  V/cm,  $B = 4$  G,  $\epsilon_z = 1$ , and  $\epsilon_x = \epsilon_i = 0$ . With  $E = 0$  V/cm the transition rates from Eq. (2.23) are

$$| (M1)_{Fm_F}^{F\pm 1m'_F} |^2 \simeq (M \mp M_{\text{hf}})^2 \Lambda^{M1}(I, \nu) (C_{Fm_F}^{F\pm 1m'_F})^2. \quad (2.28)$$

With  $E \simeq 700$  V/cm, [using Eq. (2.18)] they are

$$| (E1_{\text{Stark}})_{Fm_F}^{F\pm 1m'_F} |^2 \simeq \beta^2 E^2 \Lambda^{E1}(I, \nu) (C_{Fm_F}^{F\pm 1m'_F})^2. \quad (2.29)$$

Here again,  $\Lambda(I, \nu)$  is a line shape factor. The total rate for a given transition is found by summing over  $m_F$  and integrating over all  $\nu$ . If we take the ratio of the total of these two rates, we have

$$R^\pm \equiv \left( \frac{M \mp M_{\text{hf}}}{\beta E} \right)^2. \quad (2.30)$$

These two ratios can be combined with a semi-empirical value of  $M_{\text{hf}}$  [27] to determine  $\beta$ .

## 2.8 Zeeman Effect in Cesium

### 2.8.1 Effect on Eigenstates

The presence of a dc magnetic field mixes the hyperfine states and shifts the energies of the  $2F + 1$  Zeeman sublevels. For a small magnetic field, the effect can be treated as a perturbation, and the Hamiltonian is given by

$$H_Z = \frac{\mu_B}{\hbar} (\hat{L} + g_S \hat{S}) \cdot \vec{B} = \frac{\mu_B}{\hbar} g_S \hat{S} \cdot \vec{B}, \quad (2.31)$$

for  $L = 0$  states. In large magnetic fields, the different  $F$  states can be mixed into one another. However, for the fields used in this thesis and in Ref. [13, 23] the mixing is on the order of or less than  $10^{-3}$  and is negligible. The energy shift for a given state is

$$\begin{aligned} \Delta\varepsilon_{nSFm_F} &= \langle nSFm_F | H_Z | nSFm_F \rangle \\ &= \mu_B g_F m_F B, \end{aligned} \quad (2.32)$$

where  $g_F$  is the Landè  $g$ -factor. For the  $F = 3$  and 4 states  $|g_F| = 4$ , so the magnitude of the frequency shift of each sublevel is given by

$$\Delta\nu_{m_F} = (0.35 \text{ MHz/G}) m_F B. \quad (2.33)$$

### 2.8.2 Effect on Spectrum

While the mixing of states due to an external magnetic field is negligible, the energy shifts due to the Zeeman effect have profound implications for PNC measurements and for the other measurements presented in this thesis. It is this shift in energy that made the 1988 PNC measurement [31] possible by completely resolving different  $6SFm_F \rightarrow 7SF'm'_F$  transitions in a large field. In the 1997 PNC measurement [13], the magnetic field was smaller but the atomic beam was spin polarized.

Therefore, the Zeeman splitting allowed a correction for unwanted transitions that would not be possible without energy shifts. For the experiments described in this thesis, no discrimination is made between different Zeeman sublevels, so the energy shifts serve only to broaden the spectral features observed. In the absence of a magnetic field, there are only the four hyperfine transitions described in Section 2.7. These are shown in Fig. 2.3. The widths of these transitions will depend on, for

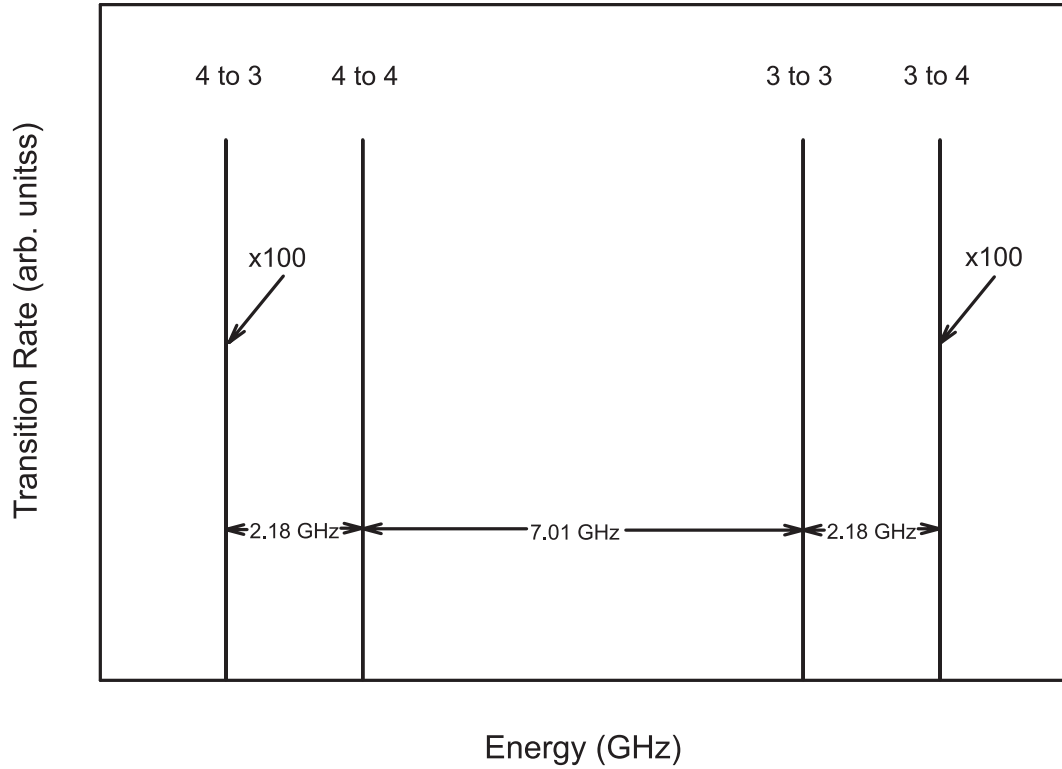
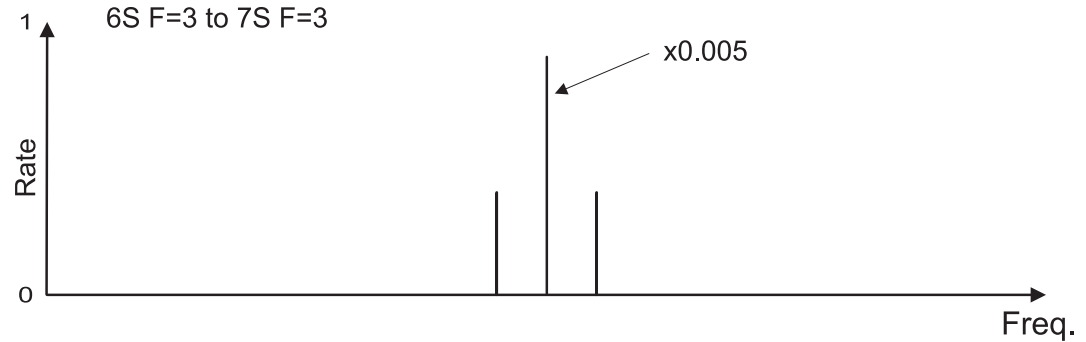


Figure 2.3: The four  $6S \rightarrow 7S$  Stark-induced electric dipole hyperfine transitions in atomic cesium in the absence of an external magnetic field.

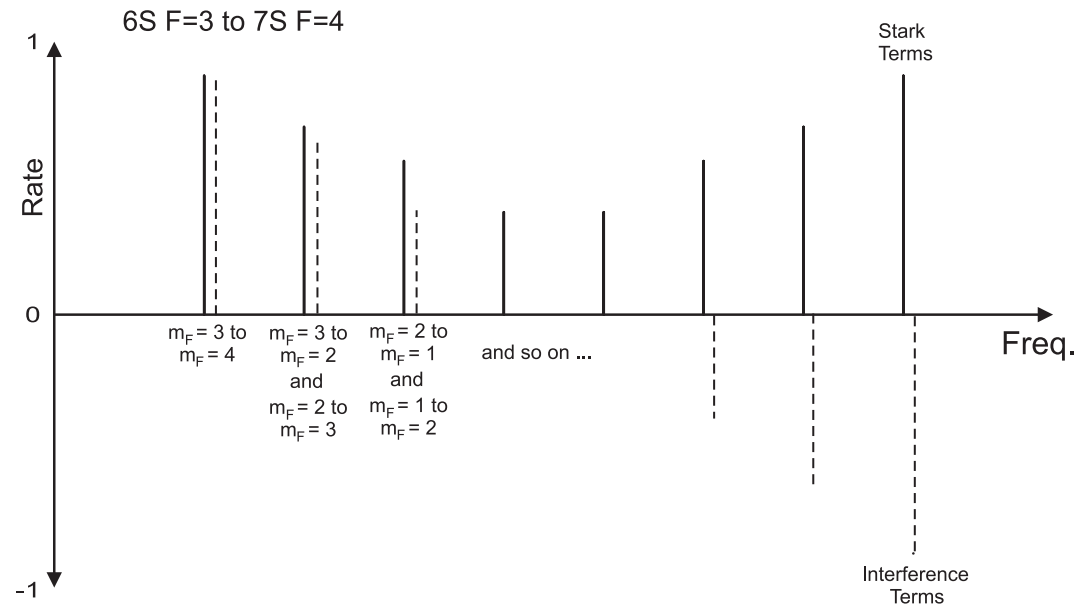
example, the Doppler width of the atomic beam or the intracavity intensity of the excitation laser.

In the presence of a magnetic field, the spectrum becomes much more complicated. As the Zeeman sublevels lose their degeneracy, each  $6S \rightarrow 7S$  hyperfine transition splits into its underlying Zeeman transitions. For  $\Delta F = 0$  transitions,

there are three spectral lines, one each for the  $\Delta m_F = 0, \pm 1$  transitions, as shown in Fig. 2.4(a). However, for  $\Delta F = \pm 1$  transitions, the Landè  $g$ -factors for different  $F$  levels have opposite signs. The result is the very complicated spectrum shown in Fig. 2.4(b).



(a)



(b)

Figure 2.4: The Zeeman spectrum for  $6S \rightarrow 7S$  transitions in a small magnetic field. (a) The spectrum for the  $F = 3$  to  $F = 3$  transition with the  $\Delta m_F = 0$  peak greatly reduced. (b) The spectrum for the  $F = 3$  to  $F = 4$  transition. The Stark-induced rates are shown in solid lines and the Stark-PNC interference terms are shown in dashed lines and offset for clarity.

As mentioned earlier, this separation of different transitions made the 1988 PNC measurement possible. This is because the interference terms on opposite sides of the spectrum have opposite signs, as is shown in Fig. 2.4(b). Without the Zeeman splitting, and assuming an approximately uniform distribution among the Zeeman sublevels, all the interference terms sum to zero. If optical pumping is used to spin polarize the atomic beam as in the 1997 PNC experiment, the Zeeman splitting reduces the level of precision needed when measuring the degree of spin polarization. This point will be discussed in more detail in Section 7.3.

For measuring the dc Stark shift (Chapter 4), the Zeeman effect is unimportant because we use the  $F = 3$  to  $F' = 3$  transition, where all  $\Delta m_F = q$  transitions that have the same value of  $q$  are degenerate. Here  $q = 0$  or  $\pm 1$ . For measuring  $\beta$  (Chapter 5), the Zeeman effect broadens the spectral feature but does not affect the total transition amplitudes we measure. Sample scans over the  $E1$   $F = +1$  transition with small and large  $\vec{B}$  are shown in Fig. 2.5.

In our measurement of  $\beta$  we would like to use as small a magnetic field as possible. This is because it is difficult to make scans over very large frequency ranges, and the smaller the magnetic field is, the narrower the transition will be. However, there is a systematic error that is proportional to the ratio of  $B_i/B_z$ , where  $i = x$  or  $y$ , so we compromise and use an intermediate magnetic field of 4 G.

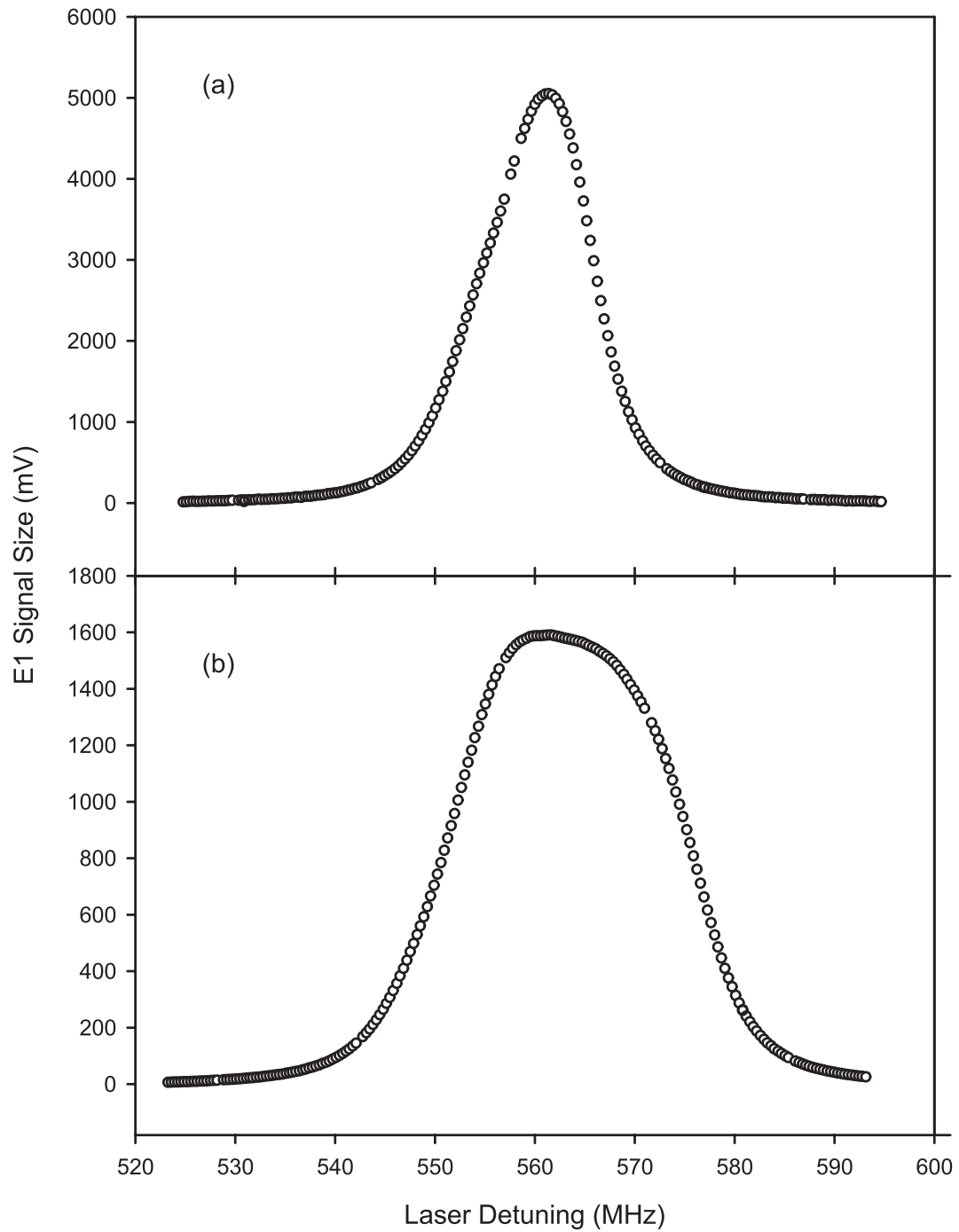


Figure 2.5: Sample scans of the  $E1$  transition in (a) small and (b) large magnetic field showing broadening due to the Zeeman effect. The total area of each transition does not change because the Zeeman effect does not change the total transition rate.